HHS Public Access

Author manuscript

Leukemia. Author manuscript; available in PMC 2023 January 01.

Published in final edited form as:

Leukemia. 2022 July ; 36(7): 1781–1793. doi:10.1038/s41375-022-01594-1.

PU.1 and MYC transcriptional network defines synergistic drug responses to KIT and LSD1 inhibition in acute myeloid leukemia

Brittany M. Curtiss[1,2], **Jake VanCampen**[3], **Jommel Macaraeg**[1,2], **Garth L. Kong**[1,2], **Akram Taherinasab**[1,2], **Mitsuhiro Tsuchiya**[1,2], **William M. Yashar**[1,2], **Yiu H. Tsang**[1,2], **Wesley Horton**[1,4], **Daniel J. Coleman**[1], **Joseph Estabrook**[1,5], **Theresa A. Lusardi**[1,5], **Gordon B. Mills**[1,2], **Brian J. Druker**[1,2,6], **Julia E. Maxson**[1,2,4,6], **Theodore P. Braun**[1,2,6]

[1]Knight Cancer Institute, Oregon Health & Science University, Portland, Oregon, 97239, USA

[2]Division of Oncological Sciences, Oregon Health & Science University, Portland, Oregon, 97239, USA

[3]Knight Cardiovascular Institute, Oregon Health & Science University, Portland, Oregon, 97239, USA

[4]Department of Cell, Developmental & Cancer Biology, Oregon Health & Science University, Portland, Oregon, 97239, USA

[5]Cancer Early Detection Advanced Research Center, Oregon Health & Science University, Portland, Oregon, 97239, USA

[6]Division of Hematology & Medical Oncology, Oregon Health & Science University, Portland, Oregon, 97239, USA

Abstract

Responses to kinase-inhibitor therapy in AML are frequently short-lived due to the rapid development of resistance, limiting the clinical efficacy. Combination therapy may improve initial therapeutic responses by targeting pathways used by leukemia cells to escape monotherapy. Here we report that combined inhibition of KIT and lysine-specific demethylase 1 (LSD1) produces synergistic cell death in *KIT*-mutant AML cell lines and primary patient samples. This drug combination evicts both MYC and PU.1 from chromatin driving cell cycle exit. Using a live cell biosensor for AKT activity, we identify early adaptive changes in kinase signaling following KIT inhibition that are reversed with the addition of LSD1 inhibitor via modulation of the GSK3a/b axis. Multi-omic analyses, including scRNA-seq, ATAC-seq and CUT&Tag, confirm these mechanisms in primary *KIT*-mutant AML. Collectively, this work provides rational for a clinical trial to assess the efficacy of KIT and LSD1 inhibition in patients with *KIT*-mutant AML.

Correspondence: Theodore P. Braun, Knight Cancer Institute, 3181 SW Sam Jackson Pk. Rd., KR-HEM, Portland, Oregon, 97239, braunt@ohsu.edu.

Author contributions

B.M.C., T.P.B., D.J.C., B.J.D., and J.E.M. designed research; B.M.C., J.M., A.T., M.T., Y.H.T., and T.P.B. performed research; B.M.C., T.P.B., J.V., G.L.K., W.Y., W.H., D.J.C., J.E., Y.H.T. and T.A.L. contributed new reagents/analytic tools; B.M.C., Y.H.T., G.B.M., T.P.B., B.J.D., and J.E.M. analyzed data; B.M.C. wrote manuscript; B.M.C., T.P.B., and J.E.M. reviewed and edited the manuscript.

Keywords

KIT inhibition; LSD1 inhibition; combined therapy; acute myeloid leukemia; leukemia epigenetics

Introduction

Epigenetic drugs have shown limited efficacy as monotherapy in acute myeloid leukemia (AML), with few patients demonstrating profound changes in disease volume(1–3). However, there is promising evidence showing increased efficacy when epigenetic drugs and kinase inhibitors are used in combination. Previously, we have showed that dual inhibition of JAK/STAT and an epigenetic regulator, lysine-specific demethylase 1 (LSD1) is an effective therapeutic strategy for *CEBPA/CSF3R* mutant AML(4). Inhibition of LSD1 restored differentiation-associated enhancer activity, further potentiating the action of JAK/STAT inhibitors in vitro and in vivo(4). Therefore, co-targeting of the leukemic epigenome with dual kinase and LSD1 inhibition represents a promising approach to obtain deeper and longer responses than are achieved by either drug alone(5).

Core binding factor (CBF) translocated AML shows a high degree of epigenetic similarity to *CEBPA*-mutant AML resulting in a differentiation block, yet is associated with different signaling mutations(6,7). *KIT* mutations are the most common signaling mutation in CBF AML and drive proliferation via downstream JAK/STAT and MAPK pathway activation(8–10). CBF AML alone is favorable risk, however, the presence of *KIT* mutations is associated with an increased risk of relapse(8,11). Avapritinib (BLU-285) is a KIT inhibitor that is currently approved by the US Food and Drug Administration (FDA) for advanced systemic mastocytosis and gastrointestinal stromal tumor (GIST), both of which have activating *KIT* mutations (NCT00782067, NCT02508532). With previously reported short-lived responses to therapeutic inhibition of other kinases in AML, avapritinib monotherapy is unlikely to produce durable responses in *KIT*-mutant AML(12,13). The efficacy of kinase plus LSD1 inhibition other AML subtypes provides rationale to investigate dual KIT and LSD1 inhibition in *KIT*-mutant AML.

Here, we demonstrate that LSD1 inhibition potentiates the activity of the KIT inhibitor, avapritinib, in leukemia cell lines and primary patient samples. This synergistic cytotoxicity is driven by perturbation of the MYC and PU.1 transcription factor networks, resulting in decreased expression of proliferation-associated genes. These mechanistic findings provide a basis for extending this dual therapeutic strategy into other molecularly defined subtypes of AML. Additionally, we identified key biomarkers to assess drug efficacy in *KIT*-mutant AML.

Results

Characterization of synergistic cytotoxicity following KIT and LSD1 inhibition

Combined kinase and LSD1 inhibition shows promise as a therapeutic strategy in certain molecularly defined subsets of AML(4). To assess LSD1 as a potential target in *KIT*-mutant AML, we mined the BeatAML database(14,15). *KIT*-mutant patient samples have

significantly increased expression of LSD1 compared to normal CD34+ samples (Fig. 1a). Additionally, the *KIT*-mutant cell line, Kasumi-1, has markedly higher expression of LSD1 compared to *KIT* wild type cell lines, MOLM-13 and K562 (Supplementary Fig. S1). Taken together, increased LSD1 expression may increase the sensitivity of *KIT*-mutant AML samples to LSD1 inhibition providing additional rational for combining LSD1 and KIT inhibition.

To investigate this combined therapy strategy in *KIT*-mutant AML, we performed a drug synergy analysis on *KIT*-mutant AML cell lines with KIT and LSD1 inhibitors. This revealed LSD1 inhibition, with either GSK-LSD1 or ORY-1001, had minimal effect on cell viability as a single agent, but markedly potentiated the efficacy of avapritinib (Fig. 1b–c, Supplementary. Fig. S2a). With 12 nM of ORY-1001, the IC50 of avapritinib decreased by 50% (Fig. 1d, Supplementary Fig. S2b). In SKNO-1 cells, we found significantly decreased proliferation after five days with combined LSD1 and KIT inhibition when compared to single drug treatment (Supplementary Fig. S2c). To further characterize the response to combined inhibition of KIT and LSD1, we performed a flow cytometry-based apoptosis assay in Kasumi-1 cells. After 48 hours of treatment, the combination group contained more PI+ (dead) and Annexin V+/PI− (early apoptosis) cells versus DMSO (Supplementary Fig. S2d–e). The drug combination produces a modest increase in apoptosis compared to either drug alone. In other molecular subtypes of AML, LSD1 inhibition promotes cell death through differentiation of immature AML blasts(4,16–20). We measured levels of maturation related surface markers at three timepoints to assess the temporal effect of differentiation. With flow cytometry we found CD86 levels increased over time by LSD1 inhibitor alone, whereas the other markers, CD11b and CD84, did not show a consistent trend (Supplementary Fig. S3a–c). This surface marker effect was not accompanied by significant morphologic differentiation after 72 hours of treatment (Supplementary Fig. S3d), in contrast to the effects seen in MLL-rearranged AML(19). To evaluate the potential for reversibility of the drug effect, we assessed markers of differentiation 72 hours after drug treatment, then again 72 hours after drug treatment was removed (Supplementary Fig. S4a–b). Kasumi-1 cells did not return to baseline differentiation after the LSD1 inhibitor or the combination was removed for 72 hours. Collectively, LSD1 inhibition results in some increased expression of mature surface markers, but does not appear to change the morphology of the cells following treatment.

A major concern of combination therapy is toxicity to normal tissues including the hematopoietic system. To evaluate the toxicity of this combination, we performed a hematopoietic colony forming assay using normal CD34+ cells in the presence of the single agents or the combination. LSD1 inhibition reduced colony formation by 33%, consistent with the know role of LSD1 in supporting multi-lineage hematopoiesis(21) (Fig. 1e). However, avapritinib did not depress colony formation alone and did not cause a further decrease in colony formation when combined with LSD1 inhibition. Furthermore, the drug combination failed to substantially alter the growth of leukemia cell lines without *KIT* mutations, arguing that the drug combination is specific to *KIT*-mutant cells (Fig. 1f). Additionally, to assess tolerability and toxicity of the drug combination in vivo, we treated healthy mice with avapritinib and ORY-1001 for 2 weeks. Body weight, white blood cell count, and hemoglobin did not significantly change after 2 weeks of treatment

(Supplementary Fig. S4c–e). Platelets modestly decreased in the mice exposed to dual therapy (Supplementary Fig. S4f). This response was not surprising as ORY-1001 has previously been shown to result in thrombocytopenia(1).

Overall, LSD1 inhibition potentiates the cytotoxic effect of avapritinib in *KIT*-mutant AML cell lines. This effect is specific to *KIT*-mutant cells as the drug combination has limited impact on healthy bone marrow or *KIT* wild type leukemia lines. Although there is some immunophenotypic evidence of differentiation with LSD1 inhibition, this is not modified by co-treatment with avapritinib, and is relatively modest compared with results obtained in MLL-rearranged models.

Combined KIT and LSD1 inhibition leads to repression of MYC targets and activation of PU.1 targets

To investigate the mechanism of synergy between LSD1 and KIT inhibition, we performed RNA-sequencing (RNA-seq) on Kasumi-1 cells treated with avapritinib, GSK-LSD1, or the combination. Unsupervised clustering was performed on all differentially expressed genes to assess patterns of expression (Fig. 1g; Supplementary Tables S1–S2). Clusters 2 and 3 showed increased expression with the combination compared to either single agent, whereas clusters 5 and 6 showed decreased expression with the combination (Fig. 1h–i; Supplementary Table S3). We leveraged pathway analysis to identify biological programs that could drive the different expression patterns. Clusters 1 and 2 revealed enrichment for SPI1 (PU.1) target genes, a transcription factor involved in hematopoietic differentiation (Fig. 1h)(22). Conversely, analysis of clusters 5 and 6 was highly enriched for MYC target genes, a key regulator of proliferation and cell survival (Fig. 1i)(23). Taken together, increased expression of PU.1 target genes and downregulation of MYC target genes are features of the synergistic effect of avapritinib and LSD1 inhibition.

Decreased activation of MYC bound promoters involved in cellular proliferation

To expound upon the changes in MYC target gene activity, we assessed MYC protein levels and observed a decrease with the drug combination (Supplementary Fig. S5a). Additionally, MYC overexpression resulted in decreased synergy between KIT and LSD1 inhibition, suggesting the overall level of MYC protein plays an important role in the response to drug (Supplementary Fig. S5b). Given the transcriptional impact of combined LSD1 and KIT inhibition on MYC target genes, we hypothesized MYC binding may be altered by the drug combination. To that end, we performed Cleavage Under Targets and Release Using Nuclease (CUT&RUN) to evaluate changes in MYC binding with drug treatment. While LSD1 inhibition alone modestly decreased global MYC binding, a greater decrease was observed with the drug combination (Fig. 2a). The majority of high confidence MYC peaks localized to promoter regions, suggesting MYC-dependent transcriptional regulation commonly occurs at promoters (Fig. 2b). Given the decreased transcript abundance of MYC target genes (Fig. 1h), we hypothesized that MYC would predominantly localize to the transcription start sites (TSS) of down regulated genes. Indeed, MYC is enriched at the TSSs of genes with decreased expression in response to the drug combination (Fig. 2c). With LSD1 inhibition alone and combined KIT/LSD1 inhibition, MYC binding decreases at the TSSs of down regulated genes. To assess whether this loss of MYC

binding was associated with decreased promoter activity, we assessed H3K27Ac read pileup at MYC bound promoters using cleavage under targets and tagmentation (CUT&Tag). Using H3K4me3 and H3K27Ac, we identified 9,369 active promoters (Supplementary Fig. S5c; Supplementary Table S4). With dual LSD1 and KIT inhibition there is a significant decrease in acetylation at MYC bound promoters (adj p-value < 2.2e-16) (Fig. 2d, Supplementary Fig. S5d; Supplementary Tables S5–S6). GO analysis of MYC bound promoters revealed an enrichment for proliferation related genes such as *CDK13* and several ribosomal components (Fig. 2e, Supplementary Fig. S5e; Supplementary Table S7). Altogether, combined inhibition of LSD1 and KIT results in decreased total MYC protein, a loss of MYC binding, and decreased activation of genes involved in cell growth. To test if this altered gene expression program changes cell growth and division, we used a flow cytometry-based assay to evaluate changes in cell cycle. After 24, 48, and 72 hours of treatment, the drug combination significantly decreased the percentage of cycling cells and increased the percentage of cells in G1 phase (Supplementary Fig. S6a–b). Taken together, loss of MYC activity reduces cell cycle; however, it is unclear how LSD1 and KIT inhibition contribute to decreased MYC transcription.

To gain further insight into the transcriptional control of MYC, we considered its promoter and enhancer regions. It has previously been shown in other AML models that MYC transcription is regulated by the blood enhancer cluster (BENC)(24,25). We used H3K4me1 signal and the previously annotated modules to identify the BENC in Kasumi-1 cells (Fig. 2f). Indeed, decreased acetylation was observed at the MYC promoter in Kasumi-1 cells following dual LSD1 and KIT inhibition (Fig. 2g). Acetylation signal within active BENC modules, defined by presence of H3K27Ac signal, also decreased post drug treatment (Fig. 2h–i). Decreased BENC activity may contribute to the loss of MYC expression following KIT and LSD1 inhibition. In sum, LSD1 and KIT inhibition results in loss of MYC binding and decreased acetylation of proliferation associate promoters ultimately leading to cell cycle arrest.

Combined KIT and LSD1 inhibition cause activation of GFI1 and LSD1 bound enhancers

The transcriptional response to combined KIT and LSD1 inhibition involves both repression of MYC target genes as well as activation of differentiation-associated genes. In other subtypes of AML, differentiation of AML blasts is a major driver of drug responses. A key driver of this differentiation response is displacement of the repressive transcription factor GFI1 from chromatin. GFI1 and LSD1 co-bind and pharmacologic inhibition of LSD1 results in a loss of GFI1 binding and activation of repressed enhancers of differentiation associated genes without accumulation of histone methylation(17). In Kasumi-1 cells, global H3K4me1 and H3K9me1 levels were not different after 24 h of treatment with LSD1 inhibitor (Supplementary Fig. S7a). To evaluate the role of GFI1 in the response to combined KIT and LSD1 inhibition in *KIT*-mutant AML, we assessed genome-wide binding of GFI1 and LSD1 by CUT&RUN. LSD1 binding did not globally change after treatment in any treatment condition (Supplementary Fig. S7b). GFI1 binding decreased with LSD1 inhibition, providing evidence of on target effect, and was lost to a greater degree with the drug combination (Supplementary Fig. S7c). To assess whether this loss of GFI1 binding was associated with activation of the underlying enhancers, we used CUT&Tag to identify

enhancers, marked by the presence of H3K4me1. Using this approach, we identified 4,199 active enhancers (Supplementary Fig. S5c; Supplementary Table 2). The enhancers bound by GFI1 and LSD1 showed subtle changes in the underlying H3K27Ac, however these changes were modest compared with the results seen in MLL rearranged AML treated with LSD1 inhibitors, arguing that other factors are the major drivers of the response to combined KIT and LSD1 (Supplementary Fig. S7d; Supplementary Tables S8–S9)(17). Indeed, this is consistent with the relatively modest immunophenotypic differentiation and absence of morphologic differentiation driven by drug treatment (Supplementary Fig. S3d).

LSD1 inhibition leads to loss of PU.1 at MYC enhancers

PU.1 has also been implicated as a regulator of LSD1 inhibitor responses and PU.1 target genes are featured prominently in our RNA-seq analysis(19) (Fig. 1h). We therefore performed CUT&RUN to profile the genome wide binding of PU.1 (Fig. 3a). PU.1 binding is completely lost after treatment with LSD1 inhibition without changes in total PU.1 protein (Fig. 3a, Supplemental Fig. S5a). Annotation of PU.1 binding sites revealed localization outside of promoter regions (Supplemental Fig. S8a). Regions that lost PU.1 binding after KIT and LSD1 inhibition were found to be involved in immune response processes (Supplemental Fig. S8b). To assess whether loss of PU.1 activity was sufficient to augment the cytotoxicity of KIT inhibition, we used both a pharmacologic inhibitor of PU.1 activity (DB2313) and a doxycycline-inducible short hairpin RNA (shRNA) targeting PU.1. In both instances, we found a dose-dependent increase in KIT inhibitor potency with increasing PU.1 inhibition or knockdown (KD) (Fig. 3b, Supplementary Fig. S8c–e). Bulk RNA-seq of Kasumi-1 cells treated with avapritinib and PU.1 shRNA showed a depletion of MYC target genes by gene set enrichment analysis (Fig. 3c, Supplementary Fig. S9a–b; Supplementary Tables S10–S12). The genes from this MYC target gene set showed more repression with the combination than with either drug alone (Supplemental Fig. S9c). These data demonstrate that a loss of PU.1 activity contributes to the repression of MYC target genes.

To understand how PU.1 KD regulates MYC expression, we performed CUT&Tag for H3K27Ac to look at activation of *MYC* regulatory elements. Acetylation of the *MYC* promoter significantly decreased with PU.1 KD and KIT inhibition (adj p-value = 0.03) (Fig. 3d; Supplementary Tables S13–S15). Interestingly, no PU.1 peak was identified at the *MYC* promoter. However, a PU.1 peak was identified at the annotated +26 Kb enhancer downstream of the *MYC* gene (26), which was marked by both H3K27Ac and H3K4me1 (Fig. 3d). Consistent with the global changes in PU.1 binding, PU.1 signal was lost with LSD1 inhibition at the +26 Kb *MYC* enhancer and PU.1 KD resulted in a significant loss of H3K27Ac which further decreased with KIT inhibition (adj p-value = 0.01; Fig. 3d). Interestingly, LSD1 and GFI1 are found at the *MYC* promoter, but they were not identified at the +26 Kb enhancer (Fig. 3d, Supplementary Fig. S9d). Moreover, LSD1 and PU.1 are both bound to active modules in the BENC, which loses acetylation with KIT inhibition and PU.1 KD (Fig. 3e–f). These data demonstrate that PU.1 may play a role in *MYC* transcription through downstream enhancers. When PU.1 binding is lost with LSD1 inhibition, BENC activation is reduced resulting in decreased transcription of *MYC* and its associated programs (Fig. 3g).

KIT and LSD1 inhibition decrease MYC protein levels and repress LSD1 target genes through PI3K/AKT pathway

MYC is a key regulator of cellular proliferation and survival, among other functions, thus its transcription, activation, and stability are carefully regulated(27). KIT activates both MAPK/RAS/ERK and PI3K/AKT pathways each contributing to MYC protein abundance(28). We hypothesized that KIT inhibition alters the activity of these pathways resulting in decreased MYC protein levels and reduced MYC binding. To assess the dynamics of AKT and ERK pathway signaling after combined KIT and LSD1 inhibition, we used a novel fluorescent biosensor that enables live-cell imaging of AKT and ERK pathway activity via nuclear-cytoplasmic redistribution of fluorescent target proteins Fig. 4a. We observed minimal change in ERK activity after either drug treatment, but observed notable changes in AKT activity (Fig. 4b, Supplementary Fig. S10a–c). To assess the relative contribution of each drug, we clustered cells based on their AKT dynamics then separated the clusters based on treatment group (Fig. 4b, Supplementary Fig. S10d). Cells demonstrating a steep drop in AKT activity with a gradual recovery to baseline over 24 hours were enriched for the treatment group of KIT inhibition only (Cluster 5). In contrast, LSD1 inhibition resulted in a gradual decrease of AKT activity during the observation period (Cluster 4). Combined inhibition of KIT and LSD1 resulted in the highest percentage of cells with a sharp drop in AKT activity and minimal recovery (Cluster 6). These results collectively demonstrate that KIT inhibition results in a rapid decrease in AKT activity followed by subsequent slow return to baseline. Simultaneous inhibition of LSD1 attenuates this recovery with slow dynamics, consistent with a transcriptional response to drug.

To assess the changes in these signaling pathways at the phosphoproteomic level, we performed reverse phase protein array (RPPA) on Kasumi-1 cells treated with the single drugs or the combination. CausalPath phosphoprotein activity network revealed decreased activation of AKT upstream of decreased total MYC protein (Supplementary Fig. S11a–b; Supplementary Table S16). To understand the dynamics of AKT signaling after combined KIT and LSD1 inhibition, we used a heatmap to visualize individual members of the PI3K/AKT pathway(29–31) (Fig. 5a–b; Supplementary Fig. S11c). Serine 21 of GSK3a/b is phosphorylated by AKT, resulting in inhibition of kinase activity (Fig. 5b). Active (dephosphorylated) GSK3a/b phosphorylates MYC to decrease protein abundance(32). After 1 h of treatment with KIT inhibition, total MYC protein and serine phosphorylated GSK3a/b (pS21) decreased markedly. However, with the addition of LSD1 inhibition, PI3K/AKT activity is further reduced.

As LSD1 inhibition potentiates the cytotoxic effects of avapritinib, we hypothesized that LSD1 might also interact with the KIT/AKT/GSK3a/b axis. Indeed, in glioblastoma cells (GSC11), GSK3b phosphorylates LSD1 resulting in activation(33). This finding suggests KIT inhibition could increase the activity of LSD1, potentially increasing the dependency on this pathway and rendering cells more sensitive to LSD1 inhibition. To test this, we identified two gene-sets of LSD1 responsive genes: genes that increase in expression with LSD1 inhibition (LSD1-repressed) and genes that decrease in expression with LSD1 inhibition (LSD1-activated). We then assessed gene set enrichment of these LSD1 responsive genes in cells responding to KIT inhibition. Consistent with the hypothesis

that KIT and LSD1 inhibition exert opposing effects on LSD1 target genes, we observed that avapritinib resulted in activation of LSD1-activated genes and repression of LSD1-repressed genes (Fig. 5c; Supplementary Table S17). We next compared the effect of LSD1 inhibition alone to combined KIT and LSD1 inhibition. With or without KIT inhibition, LSD1 inhibition resulted in activation of LSD1-repressed genes. However, LSD1-activated genes were only repressed by LSD1-inhibitor monotherapy but not when combined with KIT inhibition. These data support a model in which KIT inhibition suppresses MYC activity but activates LSD1 as a drug escape mechanism. This adaptive response to KIT inhibition can be targeted with the addition of LSD1 inhibitor, potentiating cell death (Fig. 5d).

We also investigated signaling responses to KIT and LSD1 inhibition at a later timepoint. At 24 hours, we observed that avapritinib-treated cells demonstrated increased levels of phospho-AKT (pS473) (Supplementary Fig. S11c, Supplementary Fig. S12a). KIT protein abundance was also upregulated with avapritinib at this time-point suggesting that upregulation of KIT may drive this later adaptive response. The addition of LSD1 inhibitor resulted in marked suppression of KIT protein abundance as well as phospho-AKT. Additionally, we found LSD1 inhibition to synergize with wortmannin, a PI3K inhibitor, which is downstream of AKT, providing additional evidence of AKT suppression playing a key role in the synergy between LSD1 and KIT inhibition (Supplementary Fig. S12b). Collectively, these results demonstrate a coordinated interplay between signaling pathways downstream of KIT (namely PI3K/AKT) and LSD1.

LSD1 and KIT inhibition is synergistically cytotoxic in KIT-mutant patient samples through MYC network repression

To verify our findings in cell lines in primary AML samples, we identified ten patient samples from the BeatAML cohort with D816 *KIT* mutations, leading to ligand independent activation that is amenable to inhibition by avapritinib(14,15). Six of those patient samples had frozen viable cells available, four of which thawed with sufficient viability for further assays (Supplementary Table S18). We elected to evaluate transcriptional and epigenetic changes at 24 hours and drug synergy after 72 hours (Fig. 6a). Of the four patient samples, three responded with synergistic cytotoxicity to the LSD1 and KIT inhibitor (Fig. 6b, Supplementary Fig. S13a–c). Sample 17-00007 was from a relapsed patient and still showed synergistic response to LSD1 and KIT inhibition (Supplementary Fig. S13b). Sample 17-01023 did not respond, but had a *KIT*-mutant VAF of 6% arguing that this mutation only exists in a small subclone (Supplementary Fig. S13b). We also tested the combination in wild type *KIT* AML patient samples, and found there was not a synergistic response to the combination of LSD1 and KIT inhibition, providing evidence for the specificity of this combination in *KIT*-mutant AML (Supplementary Fig. S13d–e). In sample 14-00613, bulk RNA-seq revealed downregulation of MYC target genes and cell cycle related genes (Fig. 6c–d; Supplementary Tables S19–S21). Log normalized counts for LSD1, KIT, SPI1, AKT1, and MYC are consistent with the changes observed in Kasumi-1 cells following drug treatment (Supplementary Fig. S13f). These transcriptional changes after dual drug treatment provide supporting evidence that suppression of MYC activity plays a key role in the response to LSD1 and KIT inhibition.

Due to the epigenetic modifying role of LSD1, we were interested to know if dual inhibition of LSD1 and KIT altered the epigenetic landscape in patient samples. We used Transposase Accessible Chromatin using sequencing (ATAC-seq) to look at changes in chromatin accessibility in sample 15-00807(34). Differential accessibility analysis revealed 1,457 regions with significantly decreased accessibility after dual LSD1 and KIT inhibition (Fig. 6e). Gene Ontology analysis of these regions revealed enrichment for genes controlling cell cycle, including *EEF2K*, a kinase involved in cell cycle(35) (adj p-value = 0.0004) (Fig. 6e, Supplementary Fig. S14a; Supplementary Tables S22–S24). In contrast, the regions of increased accessibility are enriched for activation of mature immune cells (Supplementary Fig. S14b). In order to specifically assess the epigenetic regulation of MYC we performed CUT&Tag for H3K27Ac on sample 14-00613. At active BENC modules, defined by the presence of H3K27Ac signal, we observed decreased accessibility and activation (Fig. 6f–g). For reference, all of the BENC modules are displayed in Supplementary Fig. S14c. Additionally, these dynamic regions are bound by PU.1 and LSD1 in Kasumi-1 cells (Fig. 6f). Taken together, these data suggest regulation of BENC to decrease MYC transcription is a conserved mechanism between the cell line model and *KIT*-mutant AML primary cells. In sum, LSD1 and KIT inhibition is synergistically cytotoxic to patient samples with *KIT* mutations. With these samples, we confirm MYC target and cell cycle repression through transcriptomics and epigenetic changes.

LSD1 and KIT inhibition results in decreased MYC expression along single cell differentiation trajectory

Recent work using single cell RNA sequencing (scRNA-seq) has revealed that AML cells show substantial heterogeneity in differentiation status, existing along a differentiation continuum(36). Cells at different relative positions on this trajectory may respond differently to treatment; however, these differences cannot be appreciated through bulk analysis. Therefore, we performed scRNA-seq to understand the transcriptional response of different cell populations within patient sample 14-00613. This analysis revealed seven transcriptionally-defined clusters (Fig. 7a; Supplementary Tables S25–S26). These clusters were classified using features of early, mid, and late maturation (Supplementary Fig. S15a–b). Given the evidence of *MYC* and MYC target repression as a key response to dual LSD1 and KIT inhibition, we assessed *MYC* expression across the myeloid trajectory (Fig. 7b–c). With combined KIT and LSD1 inhibition relative to DMSO control treatment, average *MYC* expression was decreased in undifferentiated cells (cluster 0) and *MYC* was detected in fewer cells. A similar response occurs in mid-trajectory cells (cluster 2). Taken together, dual inhibition of LSD1 and KIT in a *KIT*-mutant patient sample results in decreased *MYC* expression in immature cells. This single cell RNA-seq analysis further supports MYC regulation as a key driver of the response to dual LSD1 and KIT inhibition.

Discussion

This work offers mechanistic insight into the mechanism of synergy between LSD1 and KIT inhibition, providing rational for evaluating the combination in patients with *KIT*-mutant AML. The standard of care treatment for patients with *KIT*-mutant AML involves induction and consolidation with cytarabine-based chemotherapy(37). Following treatment, patients

with CBF AML harboring mutant *KIT* have higher risk of relapse compared to CBF AML alone, thus the need for improved therapeutic options(38). In this study, we evaluated dual inhibition of LSD1 and KIT as a novel combination therapy for *KIT*-mutant AML. We show that combined inhibition of LSD1 and KIT is synergistically cytotoxic to AML cell lines harboring *KIT* mutations. Bulk RNA-seq revealed dysregulation of MYC and PU.1 (SPI1) transcriptional networks following combination treatment. Dual inhibition of LSD1 and KIT resulted in a loss of MYC protein levels and binding, along with a decrease of activating H3K27Ac at cell cycle genes, driving cell cycle exit. Furthermore, we identified a previously unappreciated role for PU.1 in driving *MYC* expression. Inhibition of LSD1 results in a global loss of PU.1 binding, including loss at the +26 kb *MYC* enhancer and blood enhancer cluster (BENC). This loss of PU.1 binding results in decreased enhancer acetylation and a corresponding decrease in *MYC* gene expression driving cell cycle exit. Dual LSD1 and KIT inhibition is also cytotoxic in AML patient samples with *KIT* mutations, with transcriptional and epigenetic profiling confirming the findings from cell lines. Our studies reveal that modulation of MYC and PU.1 transcriptional networks is a key feature of dual LSD1 and KIT inhibition. These data provide pre-clinical rational for early phase clinical trials investigating this combination in *KIT*-mutant AML.

PU.1 has previously been implicated as a key determinant of LSD1 inhibitor responses in MLL-rearranged AML, with LSD1 inhibition leading to activation of PU.1 bound enhancers(17,19). Consistent with this, our RNA-seq shows that PU.1 targets are activated with combined KIT and LSD1 inhibition. Interestingly, genome wide profiling revealed a loss of PU.1 binding with LSD1 inhibition. Together these data suggest that PU.1 serves as a transcriptional repressor at a large number of genes. Depending on the context, PU.1 can act as a repressor or activator(39). In normal hematopoiesis PU.1 and RUNX1, a part of the core binding factor (CBF) complex, are coactivators; however, PU.1 and RUNX1-ETO, a CBF fusion, are corepressors(40). CBF fusions are expressed in the *KIT*-mutant AML samples used in this study. Thus, when PU.1 binding is lost due to LSD1 inhibition, it is likely reactivating genes that were repressed by PU.1/RUNX1-ETO. At other loci, our data suggest PU.1 serves as a transcriptional activator, likely through interactions with coactivators, such as histone acetyl transferases(41). In our study, PU.1 loss is accompanied by a loss of H3K27Ac at the +26 kB *MYC* enhancer and BENC with a corresponding decrease in *MYC* expression, suggesting transactivation activity. When PU.1 is knocked-down, as a model for PU.1 binding loss, we observed a decrease in acetylation at the enhancers and promoter of *MYC*. We hypothesize that loss of activating PU.1 complexes at these *MYC* enhancers leads to a loss of *MYC* expression and cell cycle exit.

The underlying mechanism of genome-wide loss of PU.1 binding in response to LSD1 inhibition is not clear, but may be regulated by co-binding and post-translational modifications. We have found regions with PU.1 and LSD1 co-binding (i.e. BENC modules) and other regions where they bind independently (i.e. *MYC* promoter and +26 kB enhancer). In the co-bound regions, PU.1 loss could be a direct result of LSD1 inhibition disrupting protein-protein interactions. However, the loss of PU.1 at regions where LSD1 is not bound, suggests an intermediate step, such as post-translational modifications. PU.1 is phosphorylated at Ser148(42,43) leading to increased activity and DNA binding. Additionally, LSD1 is known to demethylate non-histone protein substrates

and could potentially regulate transcription factors, such as PU.1, in this manner. The precise mechanism of LSD1-dependent suppression of PU.1 activity in *KIT*-mutant AML remains an important area for future investigation.

GFI1 has been identified as a repressive transcription factor that co-binds with LSD1(17). Disruption of the LSD1-GFI1 complex has been implicated as a key mechanism of LSD1 inhibitor response in MLL-rearranged AML resulting in enhancer activation and subsequent differentiation(17). We confirmed that LSD1 inhibition also evicts GFI1 from chromatin in *KIT*-mutant AML, but found that this loss of GFI1 binding did not substantially alter the activity of underlying enhancers. We did identify numerous regions of differential chromatin remodeling and gene activation in response to LSD1 inhibition, arguing that additional factors are also crucial for driving drug responses. Indeed, prior studies have nominated numerous other transcription factors as key regulators of the effect of LSD1 inhibitor including CEBPA, PU.1 and MYB(17). Our results suggest that GFI1 dependent gene regulation may play a more prominent role in MLL-rearranged AML than *KIT*-mutant AML. It is unknown if GFI1 contributes to changes in MYC and PU.1 transcriptional networks in *KIT*-mutant AML, and is a key area for future study.

Collectively, our results demonstrate dual inhibition of KIT and LSD1 is synergistically cytotoxic in *KIT*-mutant AML cell lines and primary patient samples. Given the propensity for *KIT*-mutant AML to relapse after standard of care treatment, many experts support bone marrow transplantation for such patients in first remission, although this has not yet become the standard of care. A less toxic treatment approach would be of high clinical value for patients of advanced age or with significant co-morbidities. We show here that combined KIT and LSD1 inhibition is highly effective against and specific for *KIT*-mutant AML, suggesting this approach could be added to standard of care treatment to decrease relapse rates or could be used in the salvage setting for individuals with relapsed disease not eligible for intensive chemotherapy. Furthermore, we identify changes in the PU.1 and MYC transcriptional networks as key biomarkers of drug efficacy. Assessment of the activity of these key transcriptional nodes could be a valuable correlate for on-target drug activity during clinical investigation. An important limitation of this study is the absence of data for in vivo efficacy. A PDX model of *KIT*-mutant CBF AML would be ideal, however there are no established models currently available. Nonetheless, the clinical utility of combined KIT and LSD1 inhibition is demonstrated by the use of primary *KIT*-mutant patient samples. In total, our results support the investigation of dual KIT and LSD1 inhibition in early phase clinical trials for patients with *KIT*-mutant AML.

Methods

Please see Supplementary Materials.

Data Availability

The Gene Expression Omnibus (GEO) accession number for all sequencing data reported in this paper is GSE182150. Other data generated in this study are available within the article and its supplementary data files or available from the corresponding author on reasonable request.

Code Availability

The code used in this manuscript is publicly available through the programs listed above.

Supplementary Material

Refer to Web version on PubMed Central for supplementary material.

Acknowledgements

We thank the following OHSU core facilities for their assistance: Advanced Light Microscopy, Flow Cytometry Shared Resource, Massive Parallel Sequencing Shared Resource, ExaCloud Cluster Computational Resource, and the Advanced Computing Center. Funding was provided by an American Society of Hematology Research Restart Award, an American Society of Hematology Scholar Award and 1 K08 CA245224 from NCI awarded to T.P.B. The Functional Proteomics RPPA Core is supported by MD Anderson Cancer Center Support Grant # 5 P30 CA016672-40.

Conflicts of interest:

B.J.D. -- SAB: Aileron Therapeutics, Therapy Architects (ALLCRON), Cepheid, Vivid Biosciences, Celgene, RUNX1 Research Program, EnLiven Therapeutics, Gilead Sciences (inactive), Monojul (inactive); SAB & Stock: Aptose Biosciences, Blueprint Medicines, Iterion Therapeutics, Third Coast Therapeutics, GRAIL (SAB inactive); Scientific Founder: MolecularMD (inactive, acquired by ICON); Board of Directors & Stock: Amgen; Board of Directors: Burroughs Wellcome Fund, CureOne; Joint Steering Committee: Beat AML LLS; Founder: VB Therapeutics; Clinical Trial Funding: Novartis, Bristol-Myers Squibb, Pfizer; Royalties from Patent 6958335 (Novartis exclusive license) and OHSU and Dana-Farber Cancer Institute (one Merck exclusive license). J.E.M. -- SAB: Ionis pharmaceuticals. WMY -- former employee of Abreos Biosciences, Inc. and was compensated in part with common stock options. Pursuant to the merger and reorganization agreement between Abreos Biosciences, Inc. and Fimafeng, Inc., WMY surrendered all of his common stock options in 03/2021. The other authors do not have conflicts of interest, financial or otherwise.

Financial support:

Funding was provided by an American Society of Hematology Research Restart Award, an American Society of Hematology Scholar Award and 1 K08 CA245224 from NCI awarded to T.P.B.

References

1. Salamero O, Montesinos P, Willekens C, Pérez-Simón JA, Pigneux A, Récher C et al. First-in-Human Phase I Study of Iadademstat (ORY-1001): A First-in-Class Lysine-Specific Histone Demethylase 1A Inhibitor, in Relapsed or Refractory Acute Myeloid Leukemia. J Clin Oncol 2020; 38: 4260–4273. [PubMed: 33052756]
2. Odenike O, Wolff JE, Borthakur G, Aldoss IT, Rizzieri D, Prebet T et al. Results from the first-in-human study of mivebresib (ABBV-075), a pan-inhibitor of bromodomain and extra terminal proteins, in patients with relapsed/refractory acute myeloid leukemia. J Clin Oncol 2019; 37: 7030–7030.
3. Dombret H, Preudhomme C, Berthon C, Raffoux E, Thomas X, Vey N et al. A Phase 1 Study of the BET-Bromodomain Inhibitor OTX015 in Patients with Advanced Acute Leukemia. Blood 2014; 124: 117–117.
4. Braun TP, Coblentz C, Smith BM, Coleman DJ, Schonrock Z, Carratt SA et al. Combined inhibition of JAK/STAT pathway and lysine-specific demethylase 1 as a therapeutic strategy in CSF3R/CEBPA mutant acute myeloid leukemia. Proc Natl Acad Sci 2020; 117: 13670–13679. [PubMed: 32471953]
5. Bewersdorf JP, Shallis R, Stahl M, Zeidan AM. Epigenetic therapy combinations in acute myeloid leukemia: what are the options? Ther Adv Hematol 2019; 10: 2040620718816698. [PubMed: 30719265]
6. Avellino R, Delwel R. Expression and regulation of C/EBPα in normal myelopoiesis and in malignant transformation. Blood 2017; 129: 2083–2091. [PubMed: 28179278]

7. Speck NA, Gilliland DG. Core-binding factors in haematopoiesis and leukaemia. Nat Rev Cancer 2002; 2: 502–513. [PubMed: 12094236]
8. Paschka P, Marcucci G, Ruppert AS, Mrózek K, Chen H, Kittles RA et al. Adverse Prognostic Significance of KIT Mutations in Adult Acute Myeloid Leukemia With inv(16) and t(8;21): A Cancer and Leukemia Group B Study. J Clin Oncol 2006; 24: 3904–3911. [PubMed: 16921041]
9. Brizzi MF, Dentelli P, Rosso A, Yarden Y, Pegoraro L. STAT Protein Recruitment and Activation in c-Kit Deletion Mutants. J Biol Chem 1999; 274: 16965–16972. [PubMed: 10358045]
10. Larizza L, Magnani I, Beghini A. The Kasumi-1 cell line: a t(8;21)-kit mutant model for acute myeloid leukemia. Leuk Lymphoma 2005; 46: 247–255. [PubMed: 15621809]
11. Lück SC, Russ AC, Du J, Gaidzik V, Schlenk RF, Pollack JR et al. KIT mutations confer a distinct gene expression signature in core binding factor leukaemia. Br J Haematol 2010; 148: 925–937. [PubMed: 20064158]
12. Ueyama J, Kure A, Okuno K, Sano H, Tamoto N, Kanzaki S. [Treatment with a tyrosine-kinase inhibitor of for c-KIT mutation and AML1-ETO double positive refractory acute myeloid leukemia]. Rinshō Ketsueki Jpn J Clin Hematol 2012; 53: 460–464.
13. Cairoli R, Beghini A, Morello E, Grillo G, Montillo M, Larizza L et al. Imatinib mesylate in the treatment of Core Binding Factor leukemias with KIT mutations: A report of three cases. Leuk Res 2005; 29: 397–400. [PubMed: 15725473]
14. Tyner JW, Tognon CE, Bottomly D, Wilmot B, Kurtz SE, Savage SL et al. Functional genomic landscape of acute myeloid leukaemia. Nature 2018; 562: 526–531. [PubMed: 30333627]
15. Bottomly D, Long N, Schultz AR, Kurtz SE, Tognon CE, Johnson K et al. Integrative Analysis of Drug Response and Clinical Outcome in Acute Myeloid Leukemia. Social Science Research Network: Rochester, NY, 2022 doi:10.2139/ssrn.4041405.
16. Harris WJ, Huang X, Lynch JT, Spencer GJ, Hitchin JR, Li Y et al. The histone demethylase KDM1A sustains the oncogenic potential of MLL-AF9 leukemia stem cells. Cancer Cell 2012; 21: 473–487. [PubMed: 22464800]
17. Maiques-Diaz A, Spencer GJ, Lynch JT, Ciceri F, Williams EL, Amaral FMR et al. Enhancer Activation by Pharmacologic Displacement of LSD1 from GFI1 Induces Differentiation in Acute Myeloid Leukemia. Cell Rep 2018; 22: 3641–3659. [PubMed: 29590629]
18. McGrath JP, Williamson KE, Balasubramanian S, Odate S, Arora S, Hatton C et al. Pharmacological Inhibition of the Histone Lysine Demethylase KDM1A Suppresses the Growth of Multiple Acute Myeloid Leukemia Subtypes. Cancer Res 2016; 76: 1975–1988. [PubMed: 26837761]
19. Cusan M, Cai SF, Mohammad HP, Krivtsov A, Chramiec A, Loizou E et al. LSD1 inhibition exerts its antileukemic effect by recommissioning PU.1- and C/EBPα-dependent enhancers in AML. Blood 2018; 131: 1730–1742. [PubMed: 29453291]
20. Barth J, Abou-El-Ardat K, Dalic D, Kurrle N, Maier A-M, Mohr S et al. LSD1 inhibition by tranylcypromine derivatives interferes with GFI1-mediated repression of PU.1 target genes and induces differentiation in AML. Leukemia 2019; 33: 1411–1426. [PubMed: 30679800]
21. Kerenyi MA, Shao Z, Hsu Y-J, Guo G, Luc S, O'Brien K et al. Histone demethylase Lsd1 represses hematopoietic stem and progenitor cell signatures during blood cell maturation. eLife 2013; 2: e00633. [PubMed: 23795291]
22. Moreau-Gachelin F. Spi-1/PU.1: an oncogene of the Ets family. Biochim Biophys Acta BBA - Rev Cancer 1994; 1198: 149–163.
23. Eilers M, Eisenman RN. Myc's broad reach. Genes Dev 2008; 22: 2755–2766. [PubMed: 18923074]
24. Bahr C, von Paleske L, Uslu VV, Remeseiro S, Takayama N, Ng SW et al. A Myc enhancer cluster regulates normal and leukaemic haematopoietic stem cell hierarchies. Nature 2018; 553: 515–520. [PubMed: 29342133]
25. Shi J, Whyte WA, Zepeda-Mendoza CJ, Milazzo JP, Shen C, Roe J-S et al. Role of SWI/SNF in acute leukemia maintenance and enhancer-mediated Myc regulation. Genes Dev 2013; 27: 2648–2662. [PubMed: 24285714]

26. Fishilevich S, Nudel R, Rappaport N, Hadar R, Plaschkes I, Iny Stein T et al. GeneHancer: genome-wide integration of enhancers and target genes in GeneCards. Database J Biol Databases Curation 2017; 2017. doi:10.1093/database/bax028.
27. Sears R The Life Cycle of C-Myc: From Synthesis to Degradation. Cell Cycle Georget Tex 2004; 3: 1133–7.
28. Gregory MA, Qi Y, Hann SR. Phosphorylation by Glycogen Synthase Kinase-3 Controls c-Myc Proteolysis and Subnuclear Localization*. J Biol Chem 2003; 278: 51606–51612. [PubMed: 14563837]
29. Manning BD, Toker A. AKT/PKB Signaling: Navigating the Network. Cell 2017; 169: 381–405. [PubMed: 28431241]
30. Darici S, Alkhaldi H, Horne G, Jørgensen HG, Marmiroli S, Huang X. Targeting PI3K/Akt/mTOR in AML: Rationale and Clinical Evidence. J Clin Med 2020; 9. doi:10.3390/jcm9092934.
31. Peck B, Ferber EC, Schulze A. Antagonism between FOXO and MYC Regulates Cellular Powerhouse. Front Oncol 2013; 3: 96. [PubMed: 23630664]
32. Sears R, Nuckolls F, Haura E, Taya Y, Tamai K, Nevins JR. Multiple Ras-dependent phosphorylation pathways regulate Myc protein stability. Genes Dev 2000; 14: 2501–2514. [PubMed: 11018017]
33. Zhou A, Lin K, Zhang S, Chen Y, Zhang N, Xue J et al. Nuclear GSK3β promotes tumorigenesis by phosphorylating KDM1A and inducing its deubiquitylation by USP22. Nat Cell Biol 2016; 18: 954–966. [PubMed: 27501329]
34. Buenrostro JD, Wu B, Chang HY, Greenleaf WJ. ATAC-seq: A Method for Assaying Chromatin Accessibility Genome-Wide. Curr Protoc Mol Biol 2015; 109: 21.29.1–21.29.9.
35. cdc2–cyclin B regulates eEF2 kinase activity in a cell cycle- and amino acid-dependent manner. EMBO J 2008; 27: 1005–1016. [PubMed: 18337751]
36. van Galen P, Hovestadt V, Wadsworth II MH, Hughes TK, Griffin GK, Battaglia S et al. Single-Cell RNA-Seq Reveals AML Hierarchies Relevant to Disease Progression and Immunity. Cell 2019; 176: 1265–1281.e24. [PubMed: 30827681]
37. Zhu H-H, Zhang X-H, Qin Y-Z, Liu D-H, Jiang H, Chen H et al. MRD-directed risk stratification treatment may improve outcomes of t(8;21) AML in the first complete remission: results from the AML05 multicenter trial. Blood 2013; 121: 4056–4062. [PubMed: 23535063]
38. Tarlock K, Alonzo TA, Wang Y-C, Gerbing RB, Ries R, Loken MR et al. Functional Properties of KIT Mutations Are Associated with Differential Clinical Outcomes and Response to Targeted Therapeutics in CBF Acute Myeloid Leukemia. Clin Cancer Res 2019; 25: 5038–5048. [PubMed: 31182436]
39. van Riel B, Rosenbauer F. Epigenetic control of hematopoiesis: the PU.1 chromatin connection. Biol Chem 2014; 395: 1265–1274. [PubMed: 25205721]
40. Hu Z, Gu X, Baraoidan K, Ibanez V, Sharma A, Kadkol S et al. RUNX1 regulates corepressor interactions of PU.1. Blood 2011; 117: 6498–6508. [PubMed: 21518930]
41. Bai Y, Srinivasan L, Perkins L, Atchison ML. Protein Acetylation Regulates Both PU.1 Transactivation and Igκ 3′ Enhancer Activity. J Immunol 2005; 175: 5160–5169. [PubMed: 16210620]
42. Pongubala JMR, Van Beveren C, Nagulapalli S, Klemsz MJ, McKercher SR, Maki RA et al. Effect of PU.1 Phosphorylation on Interaction with NF-EM5 and Transcriptional Activation. Science 1993; 259: 1622–1625. [PubMed: 8456286]
43. Rieske P, Pongubala JR. AKT Induces Transcriptional Activity of PU.1 through Phosphorylation-mediated Modifications within Its Transactivation Domain *. J Biol Chem 2001; 276: 8460–8468. [PubMed: 11133986]
44. Ianevski A, Giri AK, Aittokallio T. SynergyFinder 2.0: visual analytics of multi-drug combination synergies. Nucleic Acids Res 2020; 48: W488–W493. [PubMed: 32246720]
45. Council NR, Studies D on E and L, Research I for LA, Animals C for the U of the G for the C and U of L. Guide for the Care and Use of Laboratory Animals: Eighth Edition. National Academies Press, 2010.

46. Kaya-Okur HS, Wu SJ, Codomo CA, Pledger ES, Bryson TD, Henikoff JG et al. CUT&Tag for efficient epigenomic profiling of small samples and single cells. Nat Commun 2019; 10: 1930. [PubMed: 31036827]
47. Buenrostro JD, Wu B, Litzenburger UM, Ruff D, Gonzales ML, Snyder MP et al. Single-cell chromatin accessibility reveals principles of regulatory variation. Nature 2015; 523: 486–490. [PubMed: 26083756]
48. Henikoff S, Henikoff JG, Kaya-Okur HS, Ahmad K. Efficient chromatin accessibility mapping in situ by nucleosome-tethered tagmentation. eLife 2020; 9: e63274. [PubMed: 33191916]
49. Skene PJ, Henikoff S. An efficient targeted nuclease strategy for high-resolution mapping of DNA binding sites. eLife 2017; 6: e21856. [PubMed: 28079019]
50. Liu N, Hargreaves VV, Zhu Q, Kurland JV, Hong J, Kim W et al. Direct Promoter Repression by BCL11A Controls the Fetal to Adult Hemoglobin Switch. Cell 2018; 173: 430–442.e17. [PubMed: 29606353]
51. Corces MR, Buenrostro JD, Wu B, Greenside PG, Chan SM, Koenig JL et al. Lineage-specific and single-cell chromatin accessibility charts human hematopoiesis and leukemia evolution. Nat Genet 2016; 48: 1193–1203. [PubMed: 27526324]
52. Langmead B, Salzberg SL. Fast gapped-read alignment with Bowtie 2. Nat Methods 2012; 9: 357–359. [PubMed: 22388286]
53. Yashar WM, Kong G, VanCampen J, Smith BM, Coleman DJ, Carbone L et al. GoPeaks: Histone Modification Peak Calling for CUT&Tag. 2022; : 2022.01.10.475735.
54. Quinlan AR, Hall IM. BEDTools: a flexible suite of utilities for comparing genomic features. Bioinformatics 2010; 26: 841–842. [PubMed: 20110278]
55. Love MI, Huber W, Anders S. Moderated estimation of fold change and dispersion for RNA-seq data with DESeq2. Genome Biol 2014; 15: 550. [PubMed: 25516281]
56. Gu Z, Eils R, Schlesner M. Complex heatmaps reveal patterns and correlations in multidimensional genomic data. Bioinformatics 2016; 32: 2847–2849. [PubMed: 27207943]
57. Yu G, Wang L-G, He Q-Y. ChIPseeker: an R/Bioconductor package for ChIP peak annotation, comparison and visualization. Bioinformatics 2015; 31: 2382–2383. [PubMed: 25765347]
58. McLean CY, Bristor D, Hiller M, Clarke SL, Schaar BT, Lowe CB et al. GREAT improves functional interpretation of cis-regulatory regions. Nat Biotechnol 2010; 28: 495–501. [PubMed: 20436461]
59. Ramírez F, Ryan DP, Grüning B, Bhardwaj V, Kilpert F, Richter AS et al. deepTools2: a next generation web server for deep-sequencing data analysis. Nucleic Acids Res 2016; 44: W160–W165. [PubMed: 27079975]
60. Kuhn RM, Haussler D, Kent WJ. The UCSC genome browser and associated tools. Brief Bioinform 2013; 14: 144–161. [PubMed: 22908213]
61. Robinson JT, Thorvaldsdóttir H, Winckler W, Guttman M, Lander ES, Getz G et al. Integrative Genomics Viewer. Nat Biotechnol 2011; 29: 24–26. [PubMed: 21221095]
62. Li H, Durbin R. Fast and accurate short read alignment with Burrows–Wheeler transform. Bioinformatics 2009; 25: 1754–1760. [PubMed: 19451168]
63. Li H, Handsaker B, Wysoker A, Fennell T, Ruan J, Homer N et al. The Sequence Alignment/Map format and SAMtools. Bioinformatics 2009; 25: 2078–2079. [PubMed: 19505943]
64. Tarasov A, Vilella AJ, Cuppen E, Nijman IJ, Prins P. Sambamba: fast processing of NGS alignment formats. Bioinformatics 2015; 31: 2032–2034. [PubMed: 25697820]
65. Bolger AM, Lohse M, Usadel B. Trimmomatic: a flexible trimmer for Illumina sequence data. Bioinformatics 2014; 30: 2114–2120. [PubMed: 24695404]
66. Dobin A, Davis CA, Schlesinger F, Drenkow J, Zaleski C, Jha S et al. STAR: ultrafast universal RNA-seq aligner. Bioinformatics 2013; 29: 15–21. [PubMed: 23104886]
67. Kuleshov MV, Jones MR, Rouillard AD, Fernandez NF, Duan Q, Wang Z et al. Enrichr: a comprehensive gene set enrichment analysis web server 2016 update. Nucleic Acids Res 2016; 44: W90–W97. [PubMed: 27141961]

68. Subramanian A, Tamayo P, Mootha VK, Mukherjee S, Ebert BL, Gillette MA et al. Gene set enrichment analysis: A knowledge-based approach for interpreting genome-wide expression profiles. Proc Natl Acad Sci 2005; 102: 15545–15550. [PubMed: 16199517]

69. Butler A, Hoffman P, Smibert P, Papalexi E, Satija R. Integrating single-cell transcriptomic data across different conditions, technologies, and species. Nat Biotechnol 2018; 36: 411–420. [PubMed: 29608179]

70. Johnson WE, Li C, Rabinovic A. Adjusting batch effects in microarray expression data using empirical Bayes methods. Biostatistics 2007; 8: 118–127. [PubMed: 16632515]

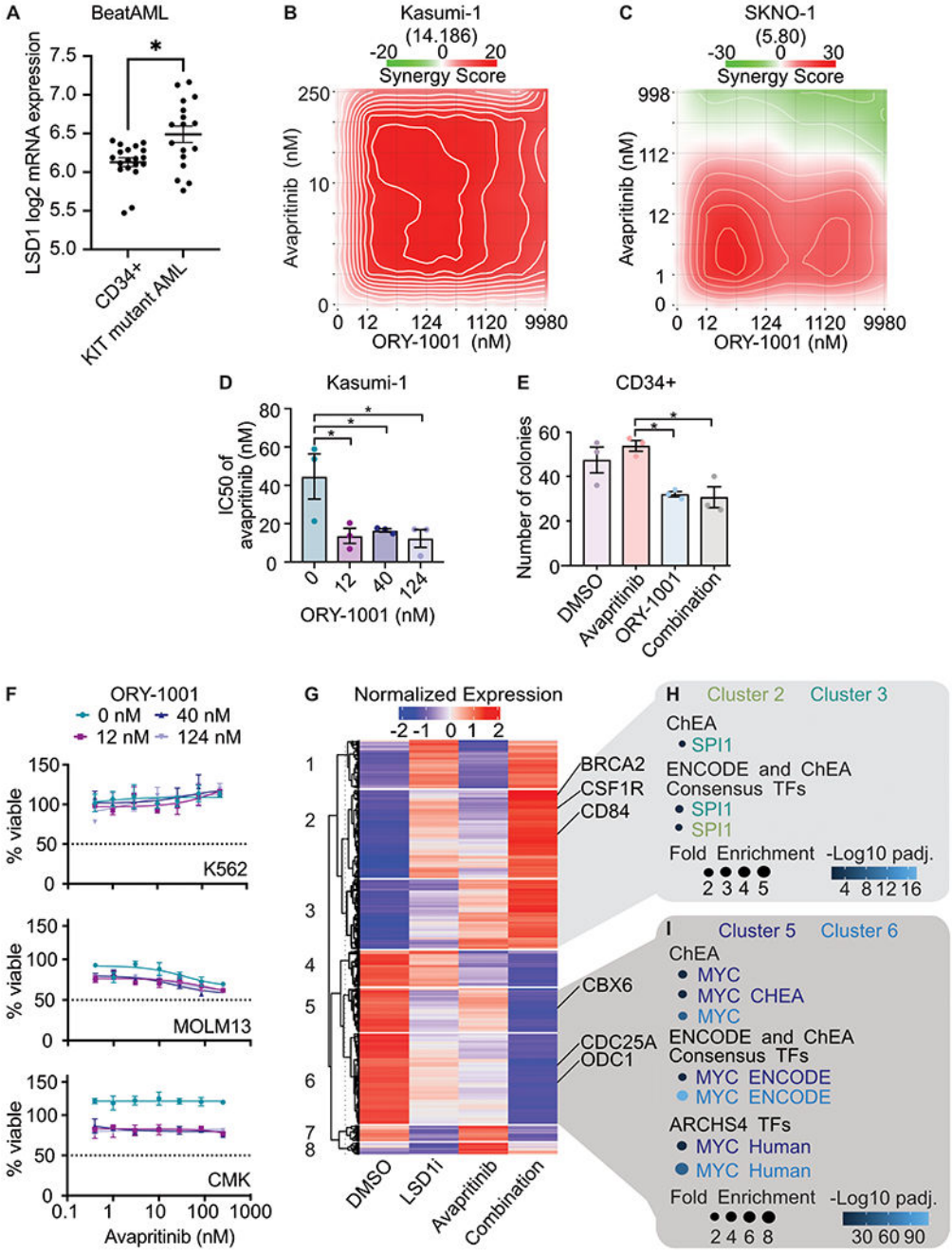

Figure 1. Synergistic cytotoxicity of dual KIT and LSD1 inhibition in a *KIT*-mutant AML cell line through activation of PU.1 and repression of MYC target genes

A. LSD1 mRNA expression in *KIT*-mutant samples from the BeatAML cohort compared with CD34+ normal controls; Mann-Whitney test (n=19 CD34+ samples and 17 *KIT*-mutant AML samples), Error bars representing SEM, * $p < 0.05$. **B.** Drug matrix of Kasumi-1 cells treated for 72 h with avapritinib and ORY-1001 with synergy assessed by zero interaction potency (ZIP) score(44). ZIP score displayed in parentheses. **C.** Drug matrix of SKNO-1 cells treated for 72 h with avapritinib and ORY-1001 with synergy assessed by ZIP score.

ZIP score displayed in parentheses. **D.** IC50 of avapritinib with different concentrations of ORY-1001 in Kasumi-1 cells treated for 72 h; one-way ANOVA with Holm-Sidak correction (n=3/group). Error bars representing SEM, *$p < 0.05$. **E.** Colony assay using healthy CD34+ cells in, treated for 14 days with avapritinib (12 nM) and/or ORY-1001 (12 nM); two-way ANOVA with Holm-Sidak correction (n=3/group). Error bars representing SEM, *$p < 0.05$. **F.** Viability assessment of K562, MOLM13, and CMK cells treated for 72 h with avapritinib and ORY-1001 (n=3/group). Error bars representing SEM. **G.** Heatmap of differentially expressed genes from RNA-seq performed on Kasumi-1 cells treated with avapritinib (12 nM) and/or GSK-LSD1 (12 nM) for 12 h (n=3/group). Genes with significant differential expression are displayed by K-means clustering. **H, I.** Gene ontology analysis of clusters 2/3 and 5/6 from F, respectively.

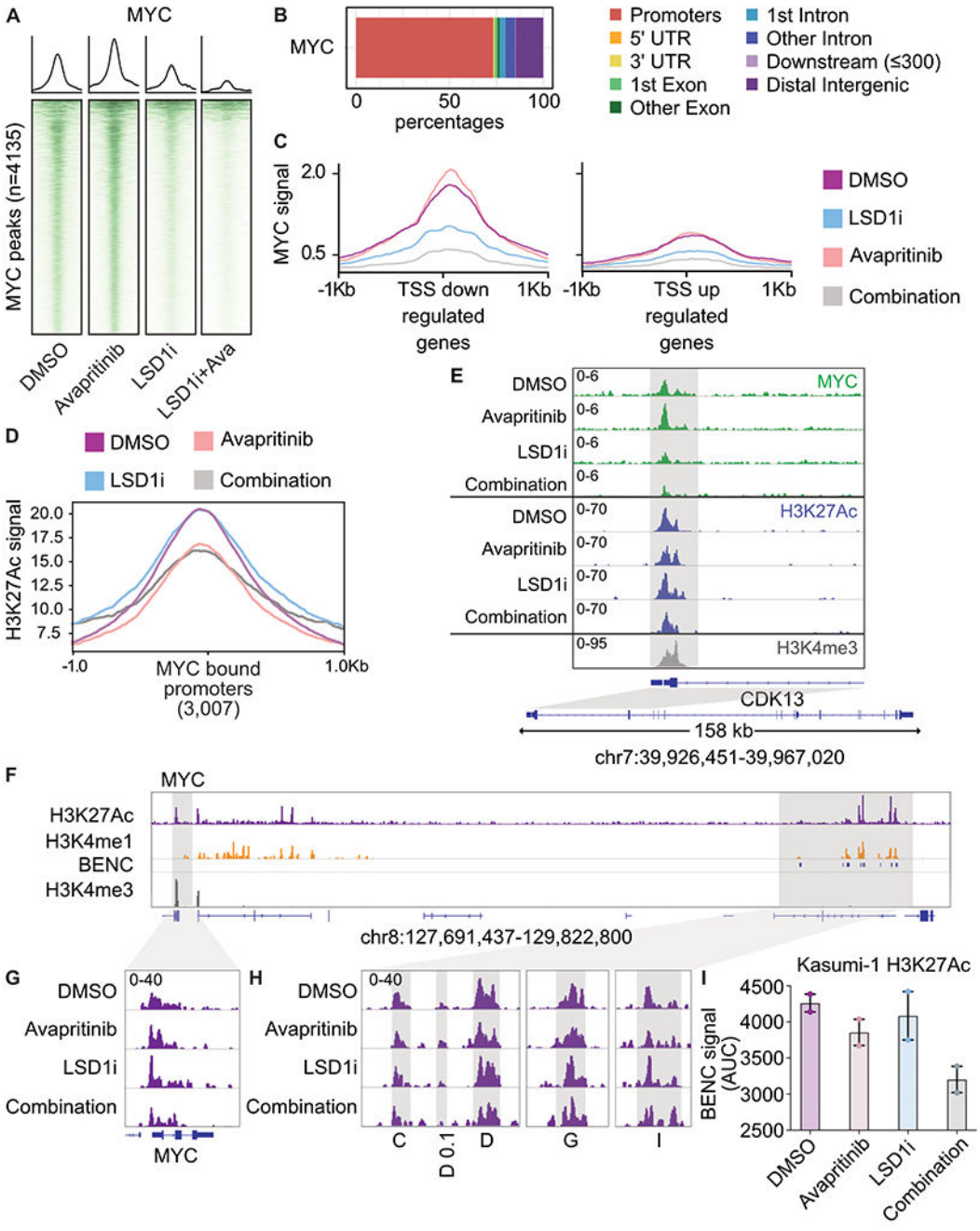

Figure 2. Repression of MYC bound promoters of cell cycle related programs.

A. Kasumi-1 cells were treated for 24 h with avapritinib (12 nM) and/or GSK-LSD1 (12 nM; LSD1i) then subject to CUT&RUN (n=2/group). Heatmaps of global signal for MYC at high confidence consensus peaks (peak apex ± 1 kb). **B.** Annotation of consensus MYC peaks. **C.** MYC signal at TSSs of down or up regulated genes defined by RNA-seq. **D.** H3K27Ac signal at all MYC bound promoters in Kasumi-1 cells after 24 h of treatment with avapritinib (12 nM) and/or GSK-LSD1 (12 nM; LSD1i). **E**. Gene ontology term enrichment for MYC bound promoters. **F.** Histone mark visualization with Integrative Genomics Viewer

(IGV) at the MYC and blood enhancer cluster (BENC) locus (n=2/group). BENC modules were identified with Kasumi-1 H3K4me1 signal that overlaps with the previously published modules(24). **G.** Histone acetylation in Kasumi-1 cells at the *MYC* locus. **H.** Histone acetylation at active BENC modules. Active BENC modules were defined by presence of H3K27Ac signal. Modules without acetylation were excluded. **I.** AUC of acetylation signal at active BENC modules.

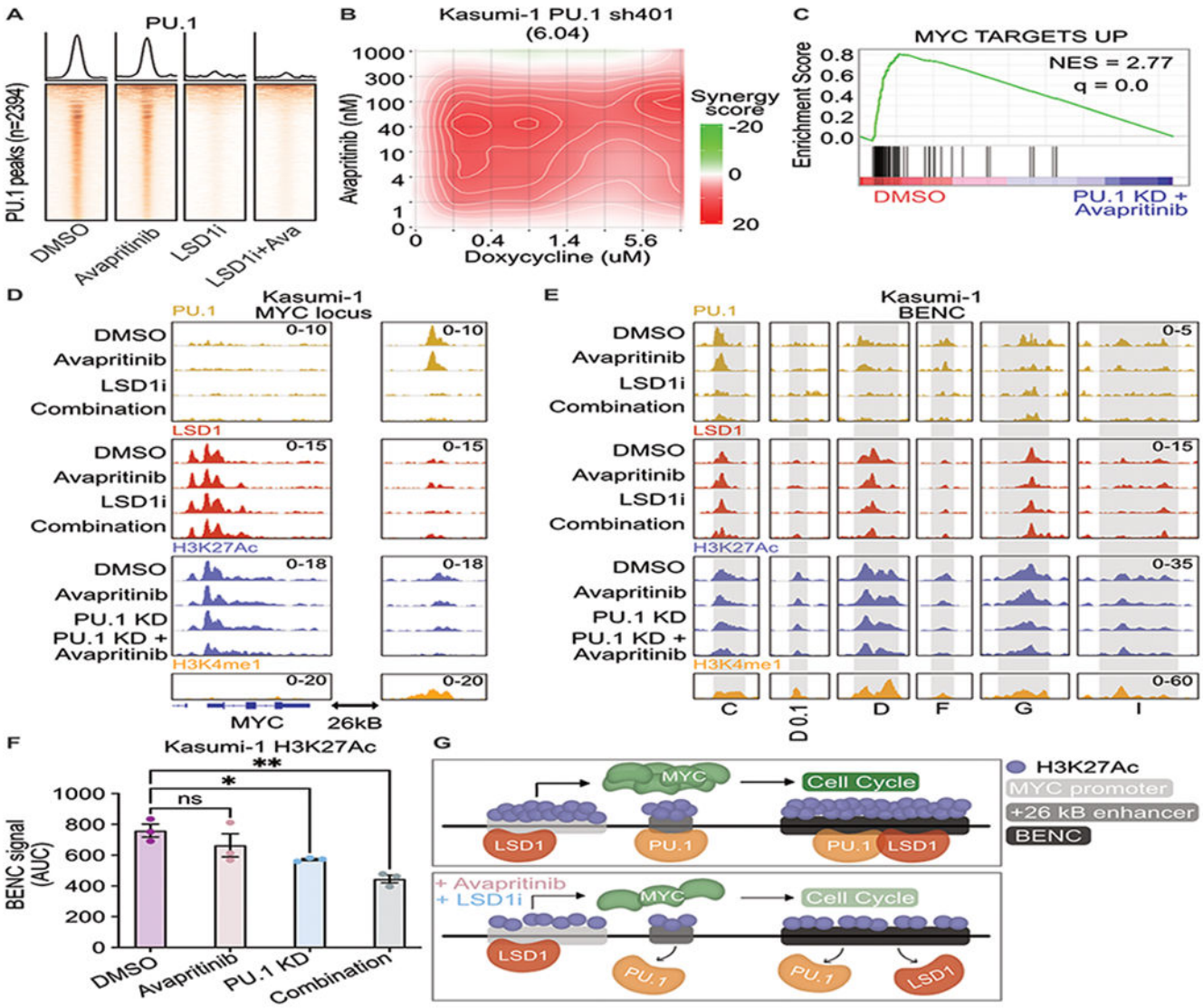

Figure 3. Loss of PU.1 binding at MYC enhancer resulting in loss of MYC enhancer and promoter activation.

A. Kasumi cells treated for 24 h with avapritinib (12 nM) and/or GSK-LSD1 (12 nM; LSD1i) then subject to CUT&RUN for PU.1 (*n*=2/group). Heatmaps of global signal for PU.1 at high confidence consensus PU.1 peaks (peak apex ± 1 kb). **B**. Drug matrix of avapritinib and doxycycline on Kasumi-1 PU.1 sh401 cells treated for 72 h. Synergy assessed by ZIP scores. ZIP score reported in parentheses. **C.** Depleted gene sets from bulk RNA-seq on PU.1 sh401, induced with doxycycline (1 μg/mL) 48 h before treatment with avapritinib (50 nM) for 24 h. NES = normalized enrichment score ($q < 0.05$). GSEA *p* value calculated by empirical permutation test and FDR adjusted. **D, E**. Kasumi-1 cells treated for 24 h with avapritinib (50 nM) and/or doxycycline (1 μg/mL) to induce PU.1 knockdown were used to perform CUT&Tag for H3K27Ac (*n*=3/group). H3K4me1, PU.1, and LSD1 signal from above datasets in Kasumi-1 cells. Visualization of +26 Kb MYC and active modules of the blood super-enhancer cluster (BENC). BENC modules are defined

Kasumi-1 H3K4me1 signal that intersects with the previously published coordinates for the BENC(24). The presence of H3K27Ac signal was used to define active modules. **F**. Quantification of cumulative AUC of H3K27Ac signal at active BENC modules; one-way ANOVA with Holms-Sidak correction. Error bars representing SEM. * $p < 0.05$, ** $p < 0.01$ **G.** Model describing loss of PU.1 binding after dual LSD1 and KIT inhibition at *MYC* +26 kB enhancer and BENC. PU.1 no longer activates *MYC* promoter resulting in decreased MYC protein, leading to decreased expression of MYC target genes including those involved with cell proliferation.

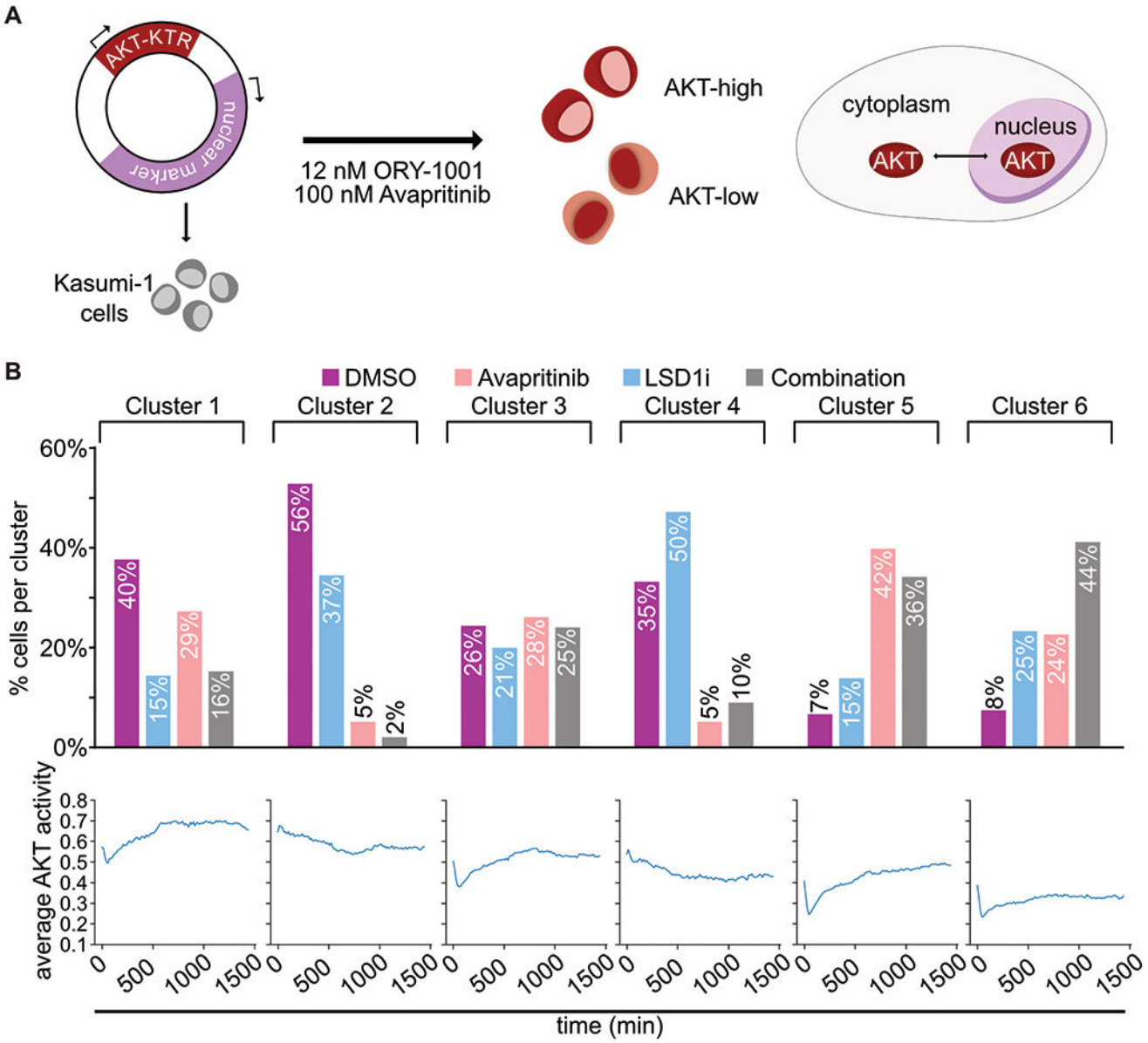

Figure 4. KIT and LSD1 inhibition attenuate AKT signaling

A. Experimental strategy to continuously assess AKT activity over time with AKT-KTR-mScarlet fluorescent biosensor. ERK activity was evaluated in the same way with ERK-KTR-Clover. B. Kasumi-1 cells were treated with avapritinib (100 nM) and/or ORY-1001 (12 nM). Subcellular localization of the fluorescent biosensors was captured with live-cell imaging. Cells were clustered based on AKT activity over time, then separated based on treatment. Bar graph displays percentage of cells from each treatment group within each cluster. Line graph displays average AKT activity over time for each cluster.

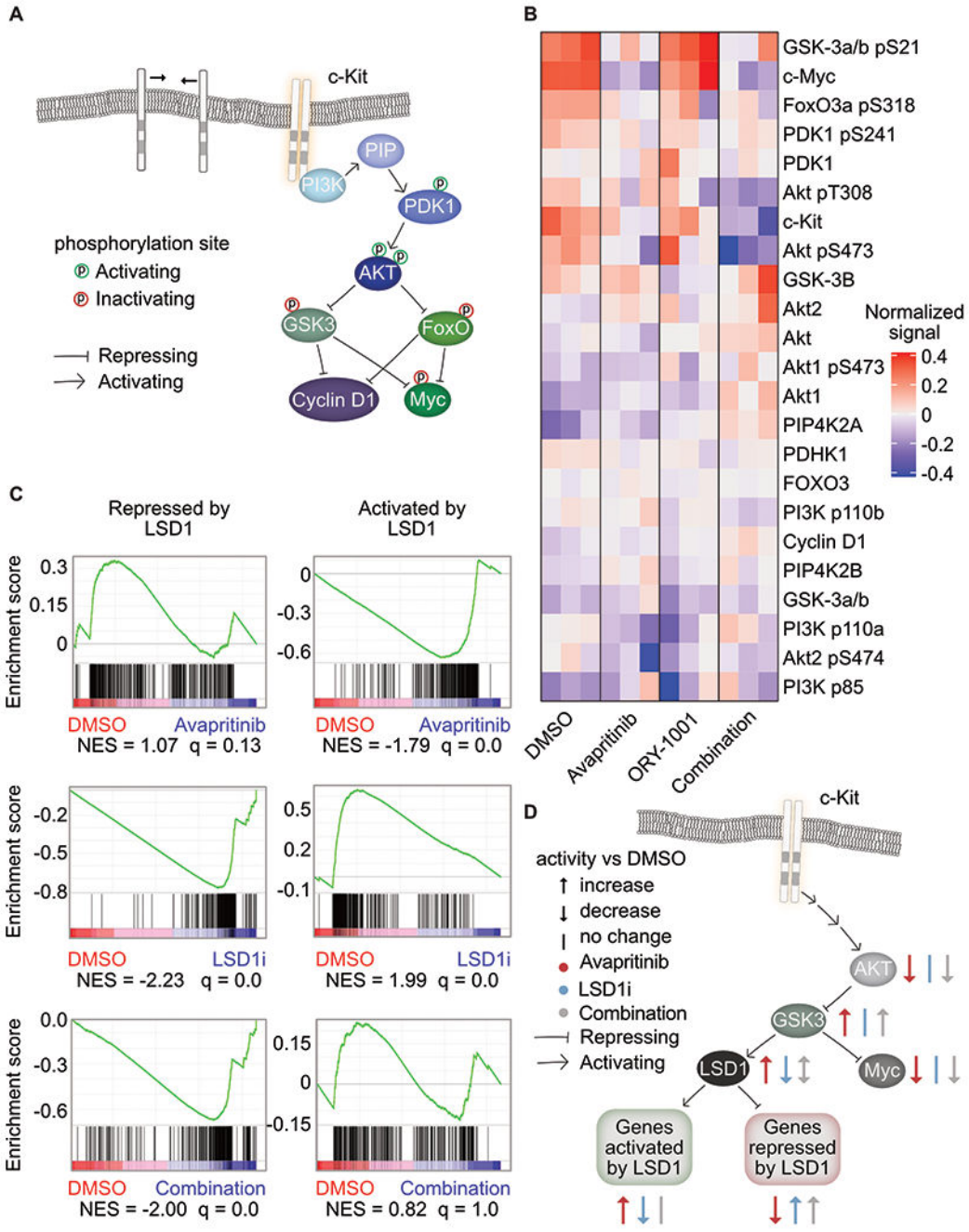

Figure 5. Coordinated PI3K/AKT signaling response to dual KIT and LSD1 inhibition

A. Depiction of PI3K/AKT signaling pathway(29–31). **B.** RPPA of Kasumi-1 cells treated for 1 h with avapritinib (100 nM) and/or ORY-1001 (12 nM). Heatmap of the normalized signal from PI3K/AKT pathway members (n=3/group). **C.** GSEA using gene sets curated by bulk RNA-seq of Kasumi-1 cells treated for 12 h with GSK-LSD1 (12 nM). Genes repressed by LSD1 have significantly increased expression after LSD1 inhibition. Genes activated by LSD1 have significantly decreased expression after LSD1 inhibition. NES = normalized enrichment score ($q < 0.05$). GSEA p value calculated by empirical permutation test and

FDR adjusted. **D.** Inhibition of KIT or LSD1 lead to opposing effect on LSD1 activity via the PI3K/AKT pathway. Dual inhibition results in repression of MYC and activation of genes natively repressed by LSD1.

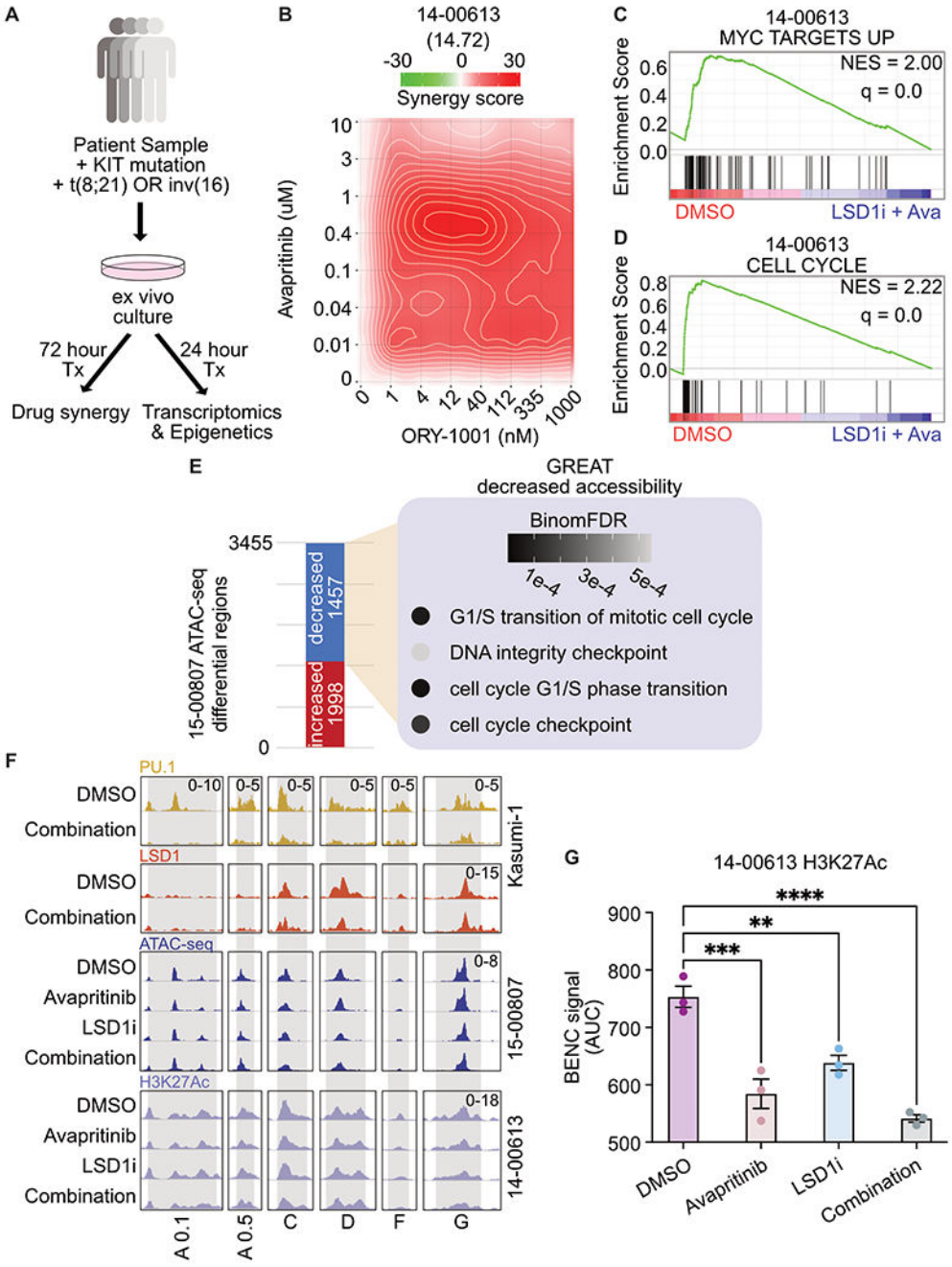

Figure 6. KIT and LSD1 inhibition synergistically target *KIT*-mutant AML patient samples resulting in decreased MYC and cell cycle programs

A. Experimental strategy for *KIT*-mutant patient samples. Frozen viable samples were cultured ex vivo and treated for 24 h before bulk RNA-seq and ATAC-seq. For synergy analysis, samples were drug treated for 72 h before assessing drug synergy. **B.** Drug matrix of patient sample 14-00613 treated for 72 h with avapritinib and ORY-1001 with synergy assessed by ZIP score. ZIP score reported in parentheses. **C, D.** Select depleted gene sets from bulk RNA-seq on 14-00613 treated with avapritinib (50 nM) and ORY-1001 (12

nM) or DMSO for 24 h. NES = normalized enrichment score ($q < 0.05$). GSEA p value calculated by empirical permutation test and FDR adjusted. **E.** Differential analysis of bulk ATAC-seq on 15-00807 treated with avapritinib (50 nM) and ORY-1001 (50 nM) compared to DMSO. Enrichment of GO terms for regions with significantly decreased accessibility. **F.** Visualization of Kasumi-1 PU.1 and LSD1 from above datasets, 15-00807 bulk ATAC-seq, and 14-00613 H3K27Ac at active BENC modules(24) (n=3/group). BENC modules defined by previously identified loci that overlap with H3K4me1 signal in Kasumi-1 cells. Active modules were designated based on presence of H3K27Ac signal. H3K27Ac CUT&Tag was performed on 14-00613 following 24 hr treatment with avapritinib (350 nM) and/or ORY-1001 (12 nM). **G.** Quantification of 14-00613 H3K27Ac signal at active BENC modules by comparing AUC; one-way ANOVA with Holm-Sidak correction. Error bars representing SEM. ** $p < 0.01$, *** $p < 0.001$, **** $p < 0.0001$

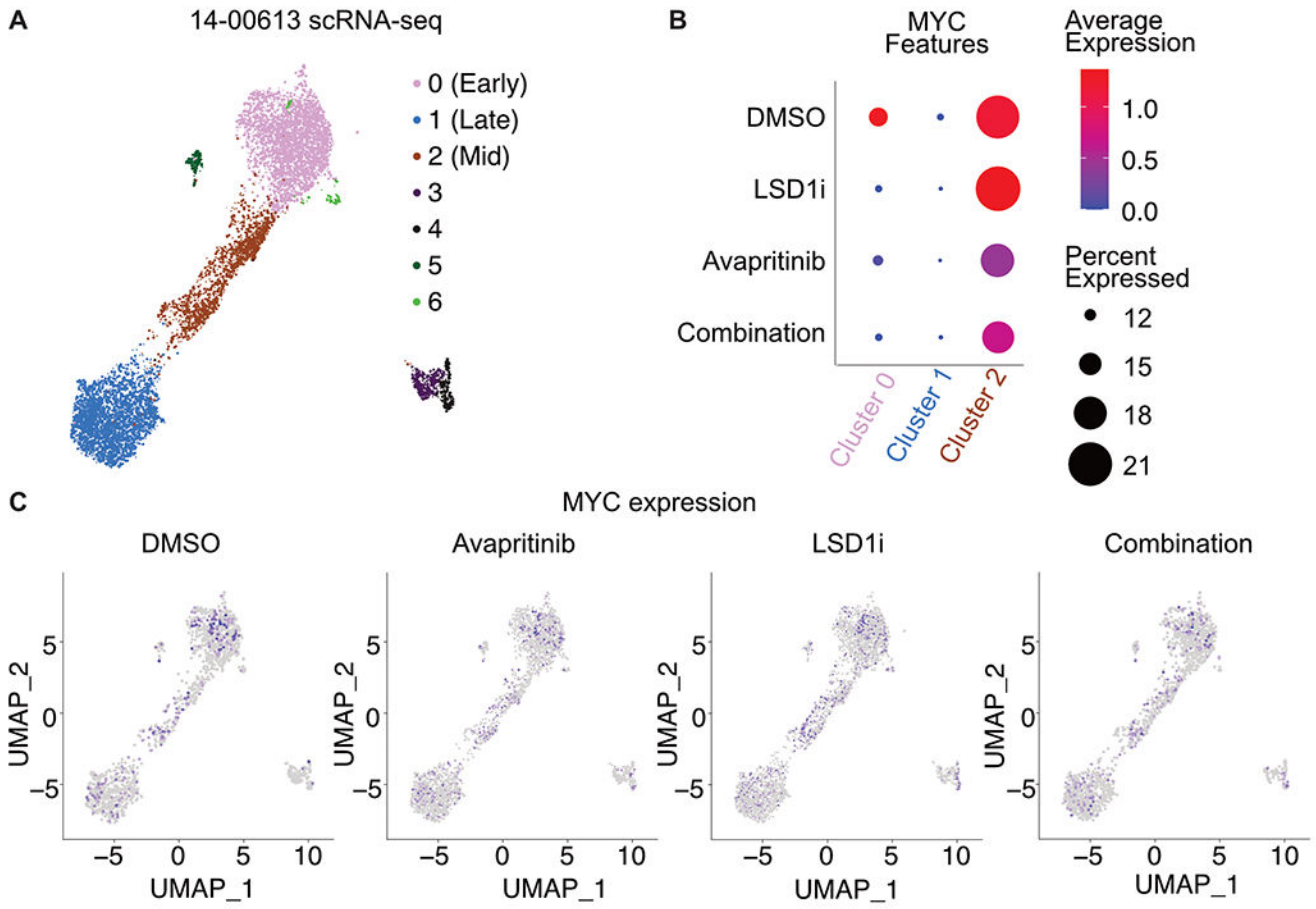

Figure 7. Varied degree of MYC loss along the differentiation trajectory post LSD1 and KIT inhibition

A. Single cell RNA-seq on patient sample 14-00613 treated with ORY-1001 (12 nM) and/or avapritinib (12 nM) for 24 h. UMAP clustering of single cell gene expression. Clustering was performed on an integrated object that included cells treated with DMSO, avapritinib, ORY-1001, or the combination. **B.** Dot plot portraying the average gene expression and percentage of cells with MYC detected per UMAP cluster in A. **C.** MYC single cell gene expression in DMSO, ORY-1001 (LSD1i), avapritinib, and the combination from single cell analysis in A.